Structure-based cleavage mechanism of *Thermus thermophilus* Argonaute DNA guide strand-mediated DNA target cleavage

Gang Sheng[a,1], Hongtu Zhao[a,b,1], Jiuyu Wang[a], Yu Rao[a], Wenwen Tian[a,b], Daan C. Swarts[c], John van der Oost[c], Dinshaw J. Patel[d,2], and Yanli Wang[a,2]

[a]Laboratory of Non-Coding RNA, Institute of Biophysics, Chinese Academy of Sciences, Beijing 100101, China; [b]University of Chinese Academy of Sciences, Beijing 100049, China; [c]Laboratory of Microbiology, Department of Agrotechnology and Food Sciences, Wageningen University, 6703 HB, Wageningen, The Netherlands; and [d]Structural Biology Program, Memorial Sloan-Kettering Cancer Center, New York, NY 10065

Contributed by Dinshaw J. Patel, November 21, 2013 (sent for review August 30, 2013)

We report on crystal structures of ternary *Thermus thermophilus* Argonaute (*Tt*Ago) complexes with 5′-phosphorylated guide DNA and a series of DNA targets. These ternary complex structures of cleavage-incompatible, cleavage-compatible, and postcleavage states solved at improved resolution up to 2.2 Å have provided molecular insights into the orchestrated positioning of catalytic residues, a pair of Mg^{2+} cations, and the putative water nucleophile positioned for in-line attack on the cleavable phosphate for *Tt*Ago-mediated target cleavage by a RNase H-type mechanism. In addition, these ternary complex structures have provided insights into protein and DNA conformational changes that facilitate transition between cleavage-incompatible and cleavage-compatible states, including the role of a Glu finger in generating a cleavage-competent catalytic Asp-Glu-Asp-Asp tetrad. Following cleavage, the seed segment forms a stable duplex with the complementary segment of the target strand.

bacterial Argonaute | catalytic mechanism | DNA guide-DNA target

Argonaute (Ago) proteins, critical components of the RNA-induced silencing complex, play a key role in guide strand-mediated target RNA recognition, cleavage, and product release (reviewed in refs. 1–3). Ago proteins adopt a bilobal scaffold composed of an amino terminal PAZ-containing lobe (N and PAZ domains), a carboxyl-terminal PIWI-containing lobe (Mid and PIWI domains), and connecting linkers L1 and L2. Ago proteins bind guide strands whose 5′-phosphorylated and 3′-hydroxyl ends are anchored within Mid and PAZ pockets, respectively (4–7), with the anchored guide strand then serving as a template for pairing with the target strand (8, 9). The cleavage activity of Ago resides in the RNase H fold adopted by the PIWI domain (10, 11), whereby the enzyme's Asp-Asp-Asp/His catalytic triad (12–15) initially processes loaded double-stranded siRNAs by cleaving the passenger strand and subsequently processes guide-target RNA duplexes by cleaving the target strand (reviewed in refs. 16–18). Such Mg^{2+} cation-mediated endonucleolytic cleavage of the target RNA strand (19, 20) resulting in 3′-OH and 5′-phosphate ends (21) requires Watson–Crick pairing of the guide and target strands spanning the seed segment (positions 2–2′ to 8–8′) and the cleavage site (10′–11′ step on the target strand) (9). Insights into target RNA recognition and cleavage have emerged from structural (9), chemical (22), and biophysical (23) experiments.

Notably, bacterial and archaeal Ago proteins have recently been shown to preferentially bind 5′-phosphoryated guide DNA (14, 15) and use an activated water molecule as the nucleophile (reviewed in ref. 24) to cleave both RNA and DNA target strands (9). Structural studies have been undertaken on bacterial and archaeal Ago proteins in the free state (10, 15) and bound to a 5′-phosphorylated guide DNA strand (4) and added target RNA strand (8, 9). The structural studies of *Thermus thermophilus* Ago (*Tt*Ago) ternary complexes have provided insights into the nucleation, propagation, and cleavage steps of target RNA silencing in a bacterial system (9). These studies have highlighted the conformational transitions on proceeding from Ago in the free state to the binary complex (4) to the ternary complexes (8, 9) and have emphasized the requirement for a precisely aligned Asp-Asp-Asp triad and a pair of Mg^{2+} cations for cleavage chemistry (9), typical of RNase H fold-mediated enzymes (24, 25). Structural studies have also been extended to binary complexes of both human (5, 6) and yeast (7) Agos bound to 5′-phosphorylated guide RNA strands.

Despite these singular advances in the structural biology of RNA silencing, further progress was hampered by the modest resolution (2.8- to 3.0-Å resolution) of *Tt*Ago ternary complexes with guide DNA (4) and added target RNAs (8, 9). This precluded identification of water molecules coordinated with the pair of Mg^{2+} cations, including the key water that acts as a nucleophile and targets the cleavable phosphate between positions 10′-11′ on the target strand. We have now extended our research

Significance

We have solved crystal structures of ternary *Thermus thermophilus* Argonaute (Ago) complexes with guide and target DNA in cleavage-incompatible, cleavage-compatible, and post-cleavage states in the 2.2- to 2.3-Å resolution range, thereby identifying the relative positions of catalytic residues, a pair of Mg^{2+} cations, and the nucleophilic water poised for in-line attack on the cleavable phosphate. These higher resolution structures represent snapshots of distinct key steps in the catalytic RNase H-mediated cleavage pathway, providing additional detailed insights into Ago-mediated cleavage chemistry of target strands. Importantly, a Glu residue shifts from an "outside" to an "inside" conformation where it inserts into the catalytic pocket to complete a catalytic tetrad during the transition from a cleavage-incompatible to a cleavage-compatible conformation.

Author contributions: Y.W. designed research; G.S., H.Z., J.W., Y.R., W.T., and Y.W. performed research; G.S., J.W., Y.R., and W.T. undertook the crystallization; H.Z. and Y.W. collected the synchrotron data; Y.W. solved the structures; D.C.S. and J.v.d.O. contributed insights on *Tt*Ago-mediated DNA guide-mediated DNA target cleavage; G.S., D.C.S., J.v.d.O., D.J.P., and Y.W. analyzed data; and D.J.P. and Y.W. wrote the paper.

The authors declare no conflict of interest.

Data deposition: The following structures have been deposited in the Protein Data Bank, www.pdb.org with accession numbers listed in parentheses: *Tt*Ago ternary complexes with 5′-phosphorylated 21-mer and added 12-mer target DNA (4N47), 15-mer target DNA (4N41), 16-mer target DNA (4NCA), and 19-mer target DNA (4NCB) for crystals grown in Mg^{2+}-containing solution; *Tt*Ago ternary complexes with 5′-phosphorylated 21-mer and added 19-mer target DNA without (4KPY) and with (4N76) preheating for 10 min at 55° C in Mn^{2+}-containing solution.

[1]G.S. and H.Z. contributed equally to this work.

[2]To whom correspondence may be addressed. E-mail: ylwang@ibp.ac.cn or pateld@mskcc.org.

This article contains supporting information online at www.pnas.org/lookup/suppl/doi:10.1073/pnas.1321032111/-/DCSupplemental.

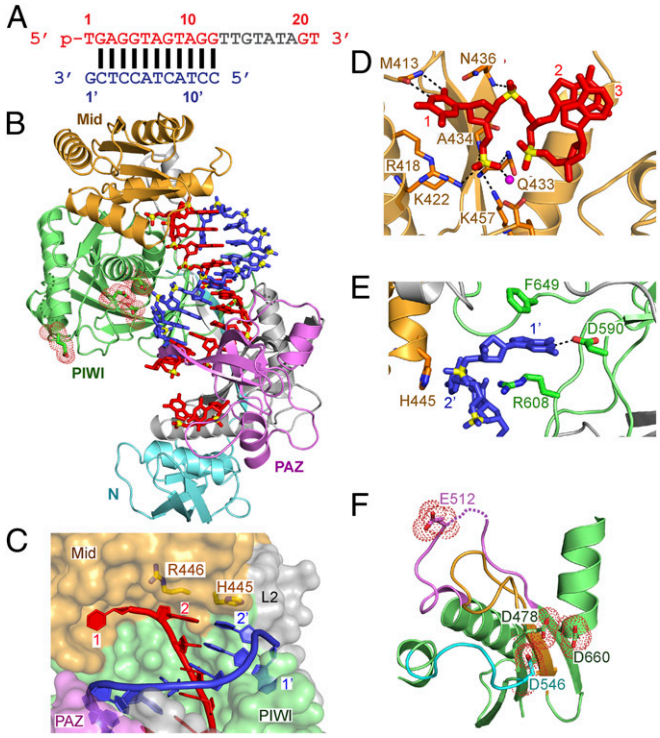

Fig. 1. Crystal structure and interactions in the *Tt*Ago ternary complex with 5′-phosphorylated 21-mer guide DNA and 12-mer target DNA complementary to segment 2–12 of the guide strand in Mg^{2+}-containing solution. (*A*) The sequence and pairing of guide (red) and target (blue) strands in the ternary complex. Disordered segments are shown in gray. (*B*) A 2.9-Å crystal structure of the complex. The various domains and linkers of *Tt*Ago are color-coded, as are the guide and target strands. The catalytic residues in a stick representation are highlighted in a red-dotted background. (*C*) A view of the guide-target segment highlighting splaying out of 1 and 1′ bases in their respective Mid and PIWI pockets in the complex. The 2–2′ base pair stacks over side chains of Arg446 and His445. (*D*) Positioning of the 5′-phosphate and sequence-specific recognition of splayed-out base T1 of the guide strand in the Mid pocket. (*E*) Positioning and sequence-specific recognition of the splayed-out base G1′ of the target strand within a pocket in the PIWI domain. (*F*) Positioning of Glu512 outside and far away from the catalytic pocket composed of Asp478, Asp546, and Asp660 residues in the ternary complex.

to *Tt*Ago ternary complexes with guide DNA and target DNA strands, which has permitted us to grow crystals of ternary complexes that diffract to higher (2.2–2.3 Å) resolution in the cleavage-incompatible, cleavage-compatible, and postcleavage steps. These high-resolution structures of *Tt*Ago ternary complexes provide snapshots of distinct key steps in the catalytic cleavage pathway, opening opportunities for experimental probing into DNA target cleavage as a defense mechanism against plasmids and possibly other mobile elements (26, 27).

Results

Ago Ternary Complexes with Target DNA in Cleavage-Incompatible State. This section outlines the structures of Ago ternary complexes with 5′-phosphorylated 21-mer guide DNA and target DNAs (12 and 15 mers in length) that adopt a cleavage-incompatible state. We have solved the 2.8-Å crystal structure of the ternary complex of *Tt*Ago bound to 12-mer target DNA (schematic in Fig. 1*A*; structure in Fig. 1*B*; X-ray statistics in *SI Appendix*, Table S1). The guide DNA strand (in red), which can be traced from positions 1–12 and 20–21, is anchored at both its ends, with the 5′-end anchored in the Mid pocket (14, 28) and the 3′-end in the PAZ pocket (29, 30). The target DNA strand (in blue) can be traced from positions 1′ to 12′, with guide-target pairing spanning base-pair positions 2–2′ to 12–12′, thereby encompassing both the seed region (base pairs 2–2′ to 8–8′) and the cleavage site (10′–11′ step on the target strand). Terminal base pair 2–2′ of the guide-target duplex is stacked over the side chains of Arg446 and His445 with bases 1 of the guide and 1′ of the target splayed out relative to the 2–2′ base pair and positioned in separate pockets in the Mid and PIWI domains, respectively (Fig. 1*C*). The positioning of the 5′-phosphate (14, 28) and sequence-specific recognition of T1 (9, 31, 32) of the guide strand in the Mid pocket is shown in Fig. 1*D* and *SI Appendix*, Fig. S1*A*. The sequence-specific recognition of G1′ on the target strand within its PIWI domain pocket is shown in Fig. 1*E* and *SI Appendix*, Fig. S1*B*.

The recent structural studies on the binary complex of yeast Ago with a bound 5′-phosphorylated guide RNA strand established that the catalytic pocket is made up of three Asp residues, with an inserted Glu completing a catalytic tetrad reflective of formation of a cleavage-compatible state (7). In the current structure of the *Tt*Ago ternary complex with 12-mer target DNA, highly conserved Glu512 is positioned outside and far from the catalytic pocket made up of Asp478, Asp546, and Asp660 (Fig. 1 *B* and *F*), indicative of the formation of a cleavage-incompatible conformation at the 12-mer target DNA level.

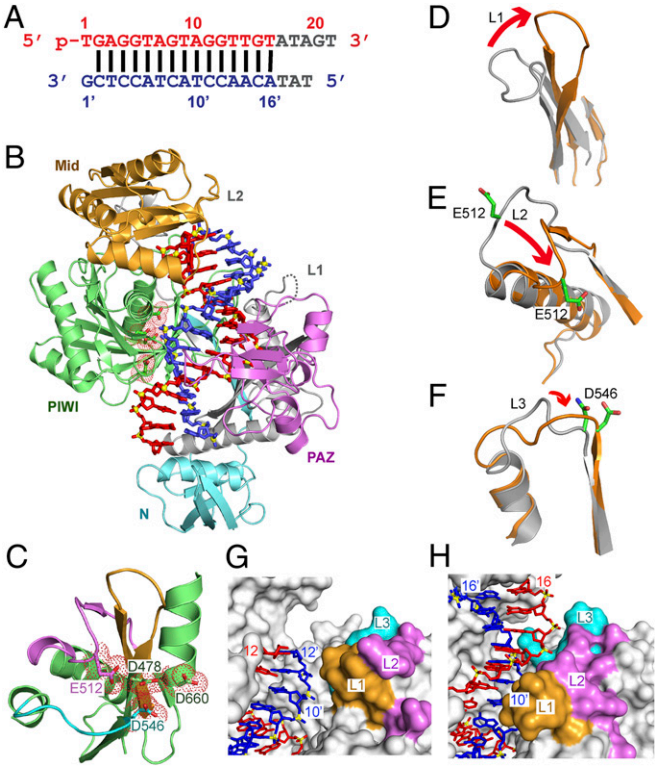

Fig. 2. Crystal structure and interactions in the *Tt*Ago ternary complex with 5′-phosphorylated 21-mer guide DNA and 19-mer target DNA complementary to segments 2–19 of the guide strand in Mg^{2+}-containing solution. (*A*) The sequence and pairing of guide (red) and target (blue) strands in the ternary complex. (*B*) A 2.2-Å crystal structure of the complex. (*C*) Insertion of Glu512 into the catalytic pocket composed of Asp478, Asp546, and Asp660 residues in the ternary complex. (*D–F*) Conformational changes in loop L1 (*D*), in loop L2 that contains Glu512 (*E*), and in loop L3 that contains Asp546 (*F*) on proceeding from the cleavage-incompatible ternary complex with 12-mer target DNA to the cleavage-compatible ternary complex with 19-mer target DNA. (*G* and *H*) Relative positioning of loops L1 (in gold), L2 (in magenta), and L3 (in cyan) in a surface representation on proceeding from the cleavage-incompatible ternary complex with 12-mer target DNA (*G*) to the cleavage-compatible ternary complex with 19-mer target DNA (*H*).

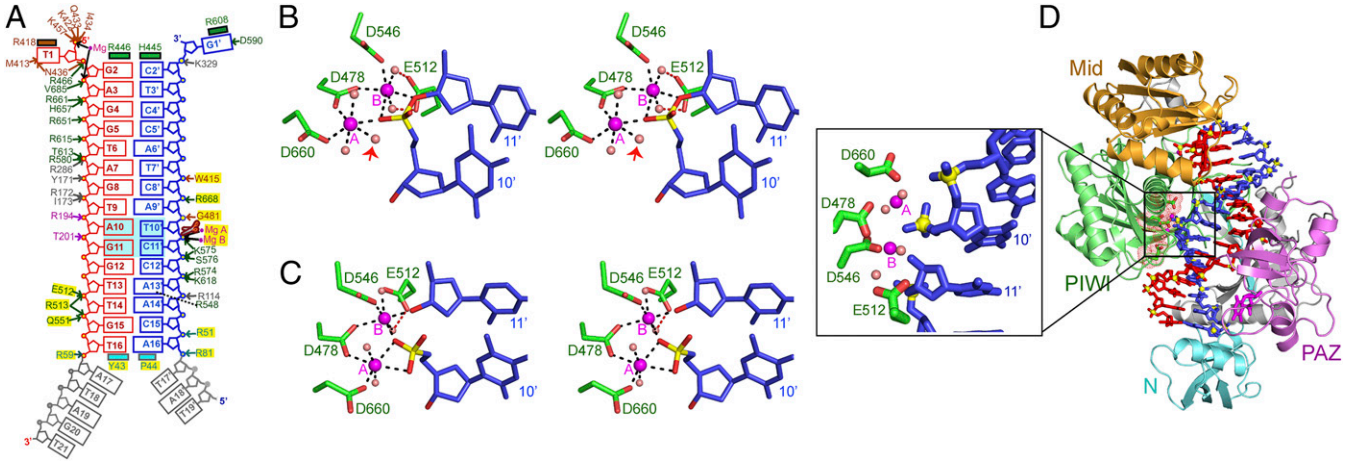

Fig. 3. Structural insights from studies of *Tt*Ago ternary complexes with 5′-phosphorylated 21-mer guide DNA and added 19-mer target DNA in the presence of Mg^{2+} and Mn^{2+}-containing solution. (*A*) Intermolecular contacts in the 2.2-Å ternary complex with cleavage-compatible 19-mer target DNA in Mg^{2+}-containing solution. The interactions highlighted by a yellow background are additional contacts observed beyond those observed in the ternary complex with cleavage-incompatible 15-mer target DNA (*SI Appendix*, Fig. S5*B*). (*B*) Stereoview of the catalytic pocket in the ternary complex with an intact 10′–11′ step on the target strand in Mg^{2+}-containing solution. The pair of Mg^{2+} cations are labeled "A" and "B" and are shown as magenta balls. Water molecules are shown as pink balls. The four catalytic Asp478, Asp546, Asp660, and Glu512 are shown in stick representation. (*C*) Stereoview of the catalytic pocket in the ternary complex with a cleaved 10′–11′ step on the target strand in Mg^{2+}-containing solution. (*D*) A 2.4-Å crystal structure and interactions in the *Tt*Ago ternary complex with 5′-phosphorylated 21-mer guide DNA and cleaved 19-mer target DNA complementary to segment 2–19 of the guide strand for crystals grown in Mn^{2+} containing solution. The target DNA is cleaved at the 10′–11′ step on the DNA target strand. The *Inset* expands the catalytic pocket segment showing the cleavage of the backbone.

We next compared the previously determined *Tt*Ago ternary complex with 12-mer target RNA (8) and the current *Tt*Ago ternary complex with 12-mer target DNA. The Ago-bound DNA–RNA (in gold) and DNA–DNA (in blue) duplexes superpose quite well (*SI Appendix*, Fig. S1*C*) with the DNA–DNA duplex (and DNA–RNA duplex), adopting a helical conformation closer to the canonical A-form (*SI Appendix*, Fig. S2*A*) than to the B-form (*SI Appendix*, Fig. S2*B*). Similarly, the Ago proteins in the two complexes (same color code) also superpose reasonably well (*SI Appendix*, Fig. S1*D*), and both adopt the cleavage-incompatible conformation, with small differences restricted to the positions of the PAZ domain (indicated by a red arrow, *SI Appendix*, Fig. S1*D*).

Ago Ternary Complex with Intact Target DNA in a Cleavage-Compatible State. This section outlines the structures of Ago ternary complexes with 5′-phosphorylated 21-mer guide DNA and target DNAs (16 and 19 mers in length) that adopt a cleavage-competent state. We have solved the 2.2-Å crystal structure of the ternary complex of *Tt*Ago bound to a 19-mer target DNA (schematic in Fig. 2*A*; X-ray statistics in *SI Appendix*, Table S2). There are two molecules of the complex in the asymmetric unit with the target DNA cleaved (between positions 10′ and 11′ with retention of the duplex on both sides of the cleavage site) in one molecule, whereas the density in the other molecule could be fit only on invoking a mixture of intact and cleaved target DNA at the 10′–11′ step (data analysis and electron density maps outlined and discussed in *SI Appendix*).

In this section, we focus on the structure of the ternary complex containing an intact 19-mer DNA target (Fig. 2*B*) and discuss the structure of the ternary complex containing the cleaved DNA target in the next section. The guide DNA strand (in red), which can be traced from positions 1–16, is anchored at its 5′-end in the Mid pocket, but the 3′-end (residues 17–21 are disordered) is positioned too far from the PAZ pocket for insertion. The target DNA strand (in blue) can be traced from positions 1′ to 16′, with guide-target pairing spanning 15 bp from base-pair position 2–2′ to 16–16′ within the nucleic acid-binding channel, with this duplex also adopting a helical conformation closer to the canonical A-form (*SI Appendix*, Fig. S2*E*) than the B-form (*SI Appendix*, Fig. S2*F*).

Again, we compared the previously determined *Tt*Ago ternary complex with 19-mer target RNA (9) and the current *Tt*Ago ternary complex with 19-mer target DNA. The DNA–RNA and DNA–DNA duplex segments superpose reasonably well (*SI Appendix*, Fig. S3*A*), as do the Ago proteins in the two complexes, except for small differences in the PAZ domain (*SI Appendix*, Fig. S3*B*).

An important difference in the *Tt*Ago ternary complex with 19-mer target DNA (relative to the complex with 12-mer target DNA) is the transition of Glu512 over a distance of 12.8 Å into the catalytic pocket to form a tetrad with the other three catalytic Asp residues (Fig. 2 *B* and *C*), thereby representing a cleavage-compatible conformation. We observed conformational changes on proceeding from the cleavage-incompatible ternary complex with 12-mer target DNA to the cleavage-compatible complex with 19-mer DNA (see segment in red box in *SI Appendix*, Fig. S4). Specifically, large structural transitions are observed within all three loops (Fig. 2 *D–F*; loops in ternary complexes with 12- and 19-mer target DNAs are colored in silver and gold, respectively), with Glu512 positioned on loop L2 inserting into the catalytic pocket (Fig. 2*E*).

The repositioning of the three loops relative to the 10′–11′ cleavage site on the target strand is clearly visible in the surface representations of the three loops (L1 in gold, L2 in magenta, and L3 in cyan) on proceeding from the cleavage-incompatible (Fig. 2*G*, ternary complex with 12-mer target DNA) to the cleavage-compatible (Fig. 2*H*, ternary complex with 19-mer target DNA) states. Moreover, additional protein–DNA intermolecular interactions are also observed with both the guide and target strands on proceeding from the cleavage-incompatible state (shown schematically for complexes with 12-mer target DNA in *SI Appendix*, Fig. S5*A* and with 15-mer target DNA in *SI Appendix*, Fig. S5*B*) to the cleavage-compatible state (complex with 19-mer target DNA, Fig. 3*A*).

In essence, release of the 3′-end of the guide strand from the PAZ pocket during the propagation step is accompanied by conformational transitions in loops 1, 2, and 3 with loop 2 residues, especially E512, forming stabilizing interactions on formation of the "inside" conformation. Such stabilization provides the driving force to shift E512 from the "outside" to the inside conformation, thereby positioning it in the catalytic pocket to complete tetrad formation.

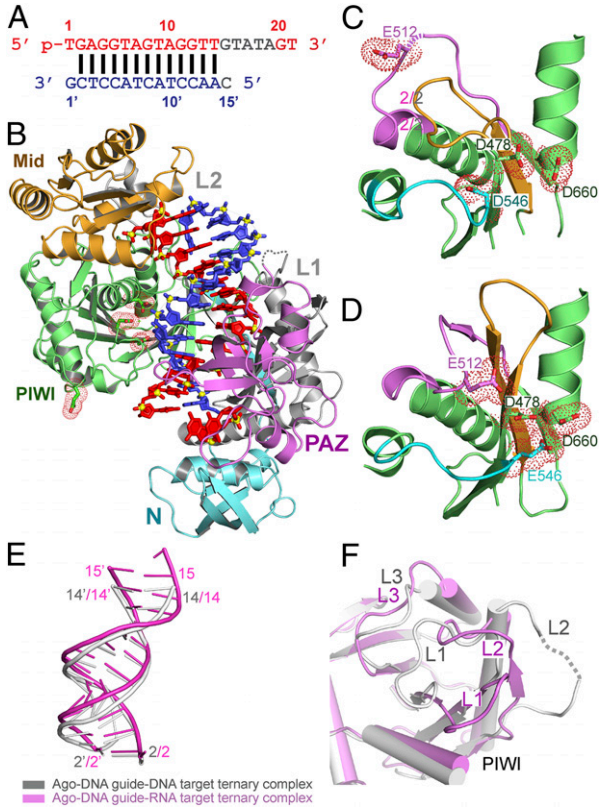

Fig. 4. Crystal structure and interactions in the *Tt*Ago ternary complex with 5′-phosphorylated 21-mer guide DNA and 15-mer target DNA complementary to segments 2–15 of the guide strand in Mg^{2+}-containing solution. (*A*) The sequence and pairing of guide (red) and target (blue) strands in the ternary complex. (*B*) A 2.25-Å crystal structure of the complex. (*C*) Positioning of Glu512 outside and far away from the catalytic pocket in the ternary complex with 15-mer target DNA. (*D*) Insertion of Glu512 into the catalytic pocket in the ternary complex with 15-mer target RNA reported previously (Protein Data Bank ID code 3HJF). (*E*) Superposition of the guide DNA-target DNA (in silver) and guide DNA-target RNA (in magneta) in the *Tt*Ago ternary complexes containing 15-mer target DNAs and RNAs. Note that we observed one more base pair (15–15′) in the ternary complex with target RNA. (*F*) Superposition of the catalytic pockets and loops L1, L2, and L3 in the ternary complexes with target DNA (in silver) and target RNA (in magenta).

We observe two hydrated Mg^{2+} cations (labeled A and B) that bridge between the three catalytic Asp residues and the cleavable but intact phosphate at the 10′–11′ step on the target strand (stereoview in Fig. 3*B*) in the cleavage-compatible state of the ternary complex with 19-mer target DNA. Mg^{2+} cation A is directly coordinated with Asp478 and Asp660 to a nonbridging phosphate oxygen and three water molecules, one of which (see arrow) is poised for in-line attack on the backbone phosphate at the cleavage site (Fig. 3*B*). Mg^{2+} cation B is directly coordinated with Asp478 and Asp546, with one each of bridging and nonbridging phosphate oxygens at the cleavage site, and with two water molecules (Fig. 3*B*). Notably, the carboxylate oxygens of Glu512, the inserted catalytic residue, are not directly coordinated to either divalent cation, but rather use a pair of bridging water molecules to coordinate with Mg^{2+} cation B (Fig. 3*B*). Given the 2.2-Å resolution of this complex, we can readily trace the Mg^{2+}-coordinated water molecules, including the proposed nucleophilic water molecule within omit maps showing the positions of water molecules (*SI Appendix*). The coordination geometries around Mg^{2+} cations A and B for the intact ternary complex are shown in *SI Appendix*, Fig. S6*A*.

Ago Ternary Complex with Cleaved Target DNA. The ternary complex of *Tt*Ago bound to 5′-phosphorylated 21-mer guide DNA and cleaved 19-mer target DNA (between positions 10′ and 11′) is shown in Fig. 3*D*, with the cleavage-site segment magnified in the *Inset*. Importantly, we observed intact guide-target duplex segments on either side of the cleaved target DNA strand.

The divalent metal coordination geometry in the *Tt*Ago ternary complex with cleaved 19-mer target DNA at the 10′–11′ step is shown in a stereoview in Fig. 3*C*. Mg^{2+} cation A is coordinated with Asp478 and Asp660 to a pair of nonbridging phosphate oxygens of the newly generated 5′-phosphate and two water molecules. Mg^{2+} cation B is coordinated with Asp478 and Asp546 to one nonbridging oxygen of the newly generated 5′-phosphate and the oxygen of the newly generated 3′-OH group and two water molecules. The inserted Glu512 remains coordinated with Mg^{2+} cation B through two bridging water molecules (Fig. 3*C*). The coordination geometries around Mg^{2+} cations A and B for the cleaved ternary complex are shown in *SI Appendix*, Fig. S6*B*.

We have superposed the structures encompassing the catalytic pocket of *Tt*Ago ternary complexes containing intact (in gold) and cleaved (blue) DNA target sites with the superposition shown in stereo in *SI Appendix*, Fig. S7.

We also grew crystals of the *Tt*Ago ternary complex with added 19-mer target DNA in Mn^{2+}-containing solution under two different conditions. Our choice of Mn^{2+} reflected the preference for Mn^{2+} over Mg^{2+} as a divalent cation for cleavage (15). The 2.4-Å crystals of the ternary complex grown in Mn^{2+}-containing solution yielded a structure (X-ray statistics in *SI Appendix*, Table S3) similar to that reported above for the cleaved structure of the ternary complex in Mg^{2+}-containing solution (Fig. 3*D*). However, when the ternary complex in the Mn^{2+}-containing solution was incubated at 55 °C for 10 min before setting up crystallization trays, not only did the 3.0-Å crystal structure of this complex (X-ray statistics in *SI Appendix*, Table S3) show cleavage of the target DNA strand at the 10′–11′ step, but also duplex formation was retained only on the side containing the seed segment, with the guide strand also disordered beyond position 10.

Comparison of Ago Ternary Complexes with 15-mer Target DNA and RNA. The 2.25-Å crystal structure of the ternary complex of *Tt*Ago bound to 5′-phosphorylated 21-mer guide DNA and 15-mer target DNA (schematic in Fig. 4*A*; X-ray statistics in *SI Appendix*, Table S1) is shown in Fig. 4*B*. The guide DNA strand (in red), which can be traced from positions 1–14 and 20–21, is anchored at both its ends. The target DNA strand (in blue) can be traced from positions 1′ to 14′, with guide-target pairing spanning 13 bp between base-pair positions 2–2′ to 14–14′.

Importantly, in the *Tt*Ago ternary complex with 15-mer target DNA (formation of 13 bp), where the 3′-end of the guide strand is retained within the PAZ pocket, Glu512 is positioned outside and far from the catalytic pocket (Fig. 4*C*), indicative of a cleavage-incompatible conformation. By contrast, in the *Tt*Ago ternary complex with 15-mer target RNA (formation of 14 bp), where the 3′-end of the guide strand is released from the PAZ pocket (9), Glu512 is inserted into the catalytic pocket (Fig. 4*D*), indicative of a cleavage-compatible conformation. Thus, it appears that a 15-mer target strand represents the tipping point during the propagation step between cleavage-incompatible and cleavage-compatible conformations, with DNA targets of this length being cleavage-incompatible and their RNA counterparts adopting cleavage-compatible conformations. We are unclear as to the origin of this difference in behavior between 15-mer DNA and RNA targets other than to point out that the Ago ternary complex with 15-mer target DNA results in formation of a 13-bp guide DNA-target DNA duplex, and the Ago complex with 15-mer target RNA results in formation of a 14-bp guide DNA-target RNA duplex (Fig. 4*E*), both of which adopt A-like conformations.

The *Tt*Ago ternary complexes formed with 15-mer target DNA (in silver) and 15-mer target RNA (in magenta) are superposed in *SI Appendix*, Fig. S8, with the observed conformational changes in the PAZ and *N*-domains and the catalytic pocket reflective of

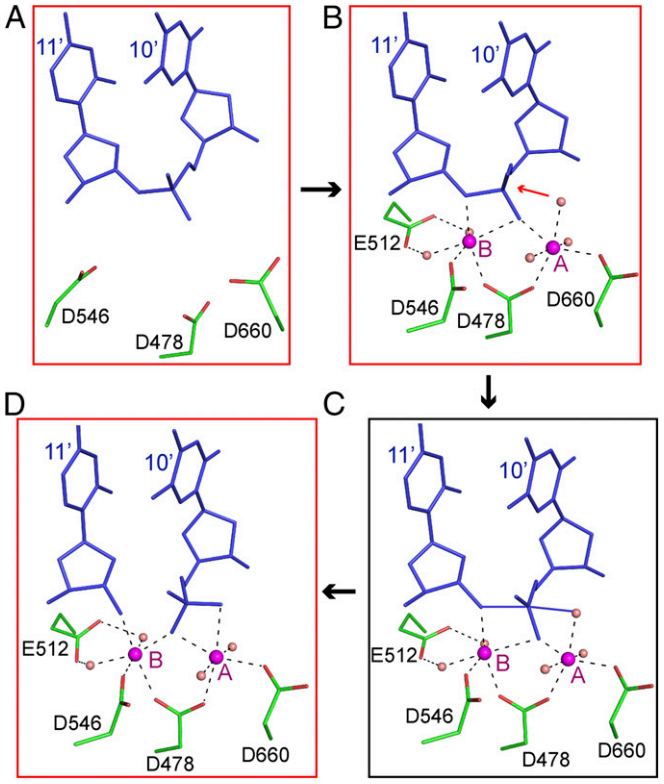

Fig. 5. A proposed mechanism for Ago-mediated Mg^{2+} cation-dependent cleavage of target strands. Crystal structure snapshots (*A*, *B*, and *D*) and a proposed model of transition state (*C*) in the reaction pathway leading to cleavage of the target DNA strand at the 10′–11′ step in the ternary complex of *Tt*Ago with complementary guide and target DNA strands. (*A*) Structure of the catalytic pocket in the cleavage-incompatible ternary complex with Glu512 positioned outside and far from the catalytic pocket as observed in ternary complexes with 12- and 15-mer target DNA strands. (*B*) Structure of the catalytic pocket in the cleavage-compatible ternary complex with Gln512 inserted into the catalytic pocket as observed in the ternary complex with 16- and 19-mer target DNA strands. (*C*) Proposed model of the transition state of the cleavage reaction in the ternary complex. (*D*) Structure of the catalytic pocket of the ternary complex following cleavage of the 10′–11′ backbone in the ternary complex with cleaved 19-mer target DNA strand.

transitions associated with conversion from cleavage-incompatible (15-mer target DNA; 13-bp formation in silver) to cleavage-compatible (15-mer target RNA; 14-bp formation in magenta) conformations (duplexes superposed in Fig. 4*E*). The conformational changes of loops L1, L2, and L3 within the catalytic pocket associated with this transition are shown in Fig. 4*F*.

We also solved the 2.5-Å structure of *Tt*Ago bound to 5′-phosphorylated guide DNA and 16-mer target DNA (X-ray statistics in *SI Appendix*, Table S2). This ternary complex formed a cleavage-compatible conformation involving formation of 15 bp of guide-target duplex similar to the ternary complex observed with the 19-mer target DNA. Thus, for *Tt*Ago ternary complexes with DNA target strands, the switch from cleavage-incompatible to cleavage-compatible complexes occurs on transition from 15-mer (formation of 13 bp) to 16-mer (formation of 15 bp) target DNA pairing with the guide DNA during the propagation step.

Discussion

Cleavage Mechanism. The PIWI domain of Ago/PIWI proteins has been shown to adopt an RNase H fold as first established from structural studies of *Pyrococcus furiosus* Ago (10) and *Archaeoglobus fulgidus* PIWI (11) in the free state. The catalytic mechanism of RNase H folds has been investigated in detail (reviewed in ref. 24) with the emphasis on factors that contribute to substrate specificity and the key contribution of a pair of Mg^{2+} cations to cleavage chemistry (33). The pair of Mg^{2+} cations, which are positioned to bridge the nucleic acid substrate and enzyme catalytic residues when properly aligned, have been proposed to greatly enhance both substrate recognition and product release, thereby enhancing catalytic efficiency. Furthermore, the scissile phosphate group projects three coordination ligands to the pair of Mg^{2+} cations in the enzyme–substrate complex. Of the pair of Mg^{2+} cations in the catalytic pocket, cation A assists in nucleophilic attack by activating a water molecule for in-line attack on the cleavable phosphate, whereas cation B stabilizes the pentacovalent intermediate and facilitates the protonation of the 3′ oxyanion-leaving group by a water molecule (reviewed in ref. 24).

Previous studies of *Tt*Ago complexes with 5′-phosphorylated guide DNA and complementary target RNAs yielded structures of ternary complexes that diffracted at best to a 2.6-Å resolution. Thus, although we were able to identify the position of Mg^{2+} cations, we were unable to identify the water molecules coordinated with these Mg^{2+} cations and hence were limited in our efforts at deducing insights into the mechanism of cleavage chemistry (9). Nevertheless, inspired by previously reported gel-based cleavage studies of *Tt*Ago ternary complexes using guide and target DNAs (9), we have attempted to improve the diffraction quality of our *Tt*Ago ternary complexes by switching from target RNAs to their target DNA counterparts. This approach has yielded higher-resolution crystals of ternary complexes that diffract to 2.25 Å (with 15-mer target DNA; Fig. 4*B*) and 2.2 Å (with 19-mer target DNA; Fig. 2*B*), thereby allowing us to identify Mg^{2+}-coordinated water molecules, including the one coordinated with Mg^{2+} cation A and positioned for in-line nucleophilic attack on the cleavable phosphate (Fig. 3*B*). Furthermore, the set of structures of ternary complexes solved in this study provide snapshots of cleavage-incompatible, cleavage-compatible, and postcleavage states, as well as the conformational transitions required for formation of a cleavage-compatible pocket.

Features of the catalytic cleavage mechanism of Ago ternary complexes with guide and target DNAs are summarized in Fig. 5. In the cleavage-incompatible conformation of the ternary complex with 12- and 15-mer target DNAs, the three catalytic Asp residues at positions 478, 546, and 660 are not properly positioned relative to the cleavable phosphate, with Glu512 positioned outside and far from the catalytic pocket and an absence of a pair of Mg^{2+} cations (Fig. 5*A*).

We highlight the following conformational changes on proceeding from the cleavage-incompatible (target DNAs of length 12–15 mer) to cleavage-compatible (target DNAs of length 16–19 mer) states. Thus, the transition from ternary complex with 15-mer target DNA (13 bp of guide-target duplex) to ternary complex with 16-mer target DNA (15 bp of guide-target duplex) during the propagation step results in the release of the 3′-end of the guide from the PAZ pocket. The accompanying conformational changes both in the guide strand and in loops L1, L2, and L3 positions Glu512 for insertion into the catalytic pocket, in the process forming a cleavage-compatible precleavage state with components held in optimal position for cleavage by two bound Mg^{2+} cations (Fig. 5*B*). The coordination geometries of Mg^{2+} cations A and B with Asp side chains, the phosphate oxygens, and coordinated waters, including the nucleophilic water poised for attack on the cleavable phosphate (shown by a red arrow Fig. 5*B*), in the precleavage structure of the complex are those characteristic of RNase H enzymes (reviewed in ref. 24). The pair of Mg^{2+} cations are separated by 3.7 Å with octahedral-like coordination geometries for Mg^{2+} cations A and B, as shown in *SI Appendix*, Fig. S6*A*. One difference is that Glu512 is coordinated with Mg^{2+} cation B through a pair of bridging water molecules in our Ago ternary complexes (Fig. 5*B*), in contrast with direct coordination with Mg^{2+} cation B in canonical RNase H enzymes (reviewed in ref. 24). Importantly, the nucleophilic water, the cleavable phosphate, and the O3 phosphate-leaving group are positioned for in-line attack to generate the proposed pentacovalent phosphate

transition state associated with an SN2 reaction with inversion of stereochemistry at the cleavable phosphate position (model of transition state shown in Fig. 5*C*).

The structure of the postcleavage state of the ternary complex is shown in Fig. 5*D*. Here again, the coordination geometries of Mg^{2+} cations A and B with Asp side chains, the phosphate oxygens, and coordinated waters are those characteristic of RNase H enzymes in the postcleavage state (reviewed in ref. 24). The pair of Mg^{2+} cations are separated by 3.6 Å, such that Mg^{2+} cation B moves toward A, with octahedral-like coordination geometries for Mg^{2+} cations A and B, as shown in *SI Appendix*, Fig. S6*B*. In our postcleavage structures of the ternary complex, Glu512 remains coordinated through two bridging water molecules to Mg^{2+} cation B.

DNA Guide Strand-Mediated DNA Target Cleavage. Our previous in vitro biochemical (9) and the current structural studies highlight the ability of bacterial Agos to use guide DNA strands to cleave target DNA strands. Such results suggest the existence of a bacterial Argonaute-mediated DNA interference pathway as a defense mechanism against transposons and mobile genetic elements, first proposed from bioinformatic studies of Ago proteins (34) and recently receiving support from molecular biology experiments (26, 27).

Materials and Methods

*Tt*Ago was prepared and purified as described previously (4) with ternary complexes generated by adding 5′-phosphorylated 21-mer guide DNA and target DNAs of varying length in the presence of divalent cations. All data sets were integrated and scaled with the HKL2000 suite (35). All structures were solved by molecular replacement with the program PHASER (36), and refined by COOT (37) and PHENIX (38). Details of crystallization, data collection, and structure determination and refinement are provided in *SI Appendix*. The refinement statistics for the ternary complexes are summarized in *SI Appendix*, Tables S1–S3.

ACKNOWLEDGMENTS. We thank the staff at beamline BL-17U at Shanghai Synchrotron Radiation Facility, beamline 3W1A at Beijing Synchrotron Radiation Facility, and beamline NE-CAT ID-24C at the Advanced Photon Source, Argonne National Laboratory. This research was funded by Chinese Ministry of Science and Technology (2011CBA01105), the Natural Science Foundation of China (31222014 and 31170705), and the Chinese Academy of Sciences (KJZD-EW-L01) (to Y.W.); and National Institutes of Health Grant AI068776 (to D.J.P.).

1. Peters L, Meister G (2007) Argonaute proteins: Mediators of RNA silencing. *Mol Cell* 26(5):611–623.
2. Hutvagner G, Simard MJ (2008) Argonaute proteins: Key players in RNA silencing. *Nat Rev Mol Cell Biol* 9(1):22–32.
3. Kawamata T, Tomari Y (2010) Making RISC. *Trends Biochem Sci* 35(7):368–376.
4. Wang Y, Sheng G, Juranek S, Tuschl T, Patel DJ (2008) Structure of the guide-strand-containing argonaute silencing complex. *Nature* 456(7219):209–213.
5. Schirle NT, MacRae IJ (2012) The crystal structure of human Argonaute2. *Science* 336(6084):1037–1040.
6. Elkayam E, et al. (2012) The structure of human argonaute-2 in complex with miR-20a. *Cell* 150(1):100–110.
7. Nakanishi K, Weinberg DE, Bartel DP, Patel DJ (2012) Structure of yeast Argonaute with guide RNA. *Nature* 486(7403):368–374.
8. Wang Y, et al. (2008) Structure of an argonaute silencing complex with a seed-containing guide DNA and target RNA duplex. *Nature* 456(7224):921–926.
9. Wang Y, et al. (2009) Nucleation, propagation and cleavage of target RNAs in Ago silencing complexes. *Nature* 461(7265):754–761.
10. Song JJ, Smith SK, Hannon GJ, Joshua-Tor L (2004) Crystal structure of Argonaute and its implications for RISC slicer activity. *Science* 305(5689):1434–1437.
11. Parker JS, Roe SM, Barford D (2004) Crystal structure of a PIWI protein suggests mechanisms for siRNA recognition and slicer activity. *EMBO J* 23(24): 4727–4737.
12. Liu J, et al. (2004) Argonaute2 is the catalytic engine of mammalian RNAi. *Science* 305(5689):1437–1441.
13. Rivas FV, et al. (2005) Purified Argonaute2 and an siRNA form recombinant human RISC. *Nat Struct Mol Biol* 12(4):340–349.
14. Ma JB, et al. (2005) Structural basis for 5′-end-specific recognition of guide RNA by the A. fulgidus Piwi protein. *Nature* 434(7033):666–670.
15. Yuan YR, et al. (2005) Crystal structure of A. aeolicus argonaute, a site-specific DNA-guided endoribonuclease, provides insights into RISC-mediated mRNA cleavage. *Mol Cell* 19(3):405–419.
16. Lingel A, Sattler M (2005) Novel modes of protein-RNA recognition in the RNAi pathway. *Curr Opin Struct Biol* 15(1):107–115.
17. Jinek M, Doudna JA (2009) A three-dimensional view of the molecular machinery of RNA interference. *Nature* 457(7228):405–412.
18. Parker JS (2010) How to slice: Snapshots of Argonaute in action. *Silence* 1(1):3.
19. Martinez J, Tuschl T (2004) RISC is a 5′ phosphomonoester-producing RNA endonuclease. *Genes Dev* 18(9):975–980.
20. Schwarz DS, Tomari Y, Zamore PD (2004) The RNA-induced silencing complex is a Mg^{2+}-dependent endonuclease. *Curr Biol* 14(9):787–791.
21. Elbashir SM, et al. (2001) Duplexes of 21-nucleotide RNAs mediate RNA interference in cultured mammalian cells. *Nature* 411(6836):494–498.
22. Ameres SL, Martinez J, Schroeder R (2007) Molecular basis for target RNA recognition and cleavage by human RISC. *Cell* 130(1):101–112.
23. Parker JS, Parizotto EA, Wang M, Roe SM, Barford D (2009) Enhancement of the seed-target recognition step in RNA silencing by a PIWI/MID domain protein. *Mol Cell* 33(2):204–214.
24. Yang W, Lee JY, Nowotny M (2006) Making and breaking nucleic acids: Two-Mg^{2+}-ion catalysis and substrate specificity. *Mol Cell* 22(1):5–13.
25. Nowotny M, Gaidamakov SA, Crouch RJ, Yang W (2005) Crystal structures of RNase H bound to an RNA/DNA hybrid: Substrate specificity and metal-dependent catalysis. *Cell* 121(7):1005–1016.
26. Olovnikov I, Chan K, Sachidanandam R, Newman DK, Aravin AA (2013) Bacterial argonaute samples the transcriptome to identify foreign DNA. *Mol Cell* 51(5):594–605.
27. Swarts D, Westra M, Brouns S, van der Oost J (2013) DNA-guided DNA interference by a prokaryotic Argonaute. *Nature*, in press.
28. Parker JS, Roe SM, Barford D (2005) Structural insights into mRNA recognition from a PIWI domain-siRNA guide complex. *Nature* 434(7033):663–666.
29. Ma JB, Ye K, Patel DJ (2004) Structural basis for overhang-specific small interfering RNA recognition by the PAZ domain. *Nature* 429(6989):318–322.
30. Lingel A, Simon B, Izaurralde E, Sattler M (2004) Nucleic acid 3′-end recognition by the Argonaute2 PAZ domain. *Nat Struct Mol Biol* 11(6):576–577.
31. Mi S, et al. (2008) Sorting of small RNAs into Arabidopsis argonaute complexes is directed by the 5′ terminal nucleotide. *Cell* 133(1):116–127.
32. Frank F, Sonenberg N, Nagar B (2010) Structural basis for 5′-nucleotide base-specific recognition of guide RNA by human AGO2. *Nature* 465(7299):818–822.
33. Steitz TA, Steitz JA (1993) A general two-metal-ion mechanism for catalytic RNA. *Proc Natl Acad Sci USA* 90(14):6498–6502.
34. Makarova KS, Wolf YI, van der Oost J, Koonin EV (2009) Prokaryotic homologs of Argonaute proteins are predicted to function as key components of a novel system of defense against mobile genetic elements. *Biol Direct* 4:29.
35. Otwinowski Z, Minor W (1997) Processing of X-ray diffraction data collected in oscillation mode. *Methods Enzymol* 276:307–326.
36. McCoy AJ, et al. (2007) Phaser crystallographic software. *J Appl Cryst* 40(Pt 4):658–674.
37. Emsley P, Cowtan K (2004) Coot: Model-building tools for molecular graphics. *Acta Crystallogr D Biol Crystallogr* 60(Pt 12 Pt 1):2126–2132.
38. Adams PD, et al. (2010) PHENIX: A comprehensive Python-based system for macromolecular structure solution. *Acta Crystallogr D Biol Crystallogr* 66(Pt 2):213–221.